Supporting Information

Laser-Induced Selective Metallization on Polymer Substrates using Organocopper for Portable Electronics

Jihai Zhang,[a,b] Jin Feng,[a] Liyang Jia,[a] Huiyuan Zhang,[a] Gaixia Zhang, [b] Shuhui Sun,[,b] and Tao Zhou*[,a]*

[a] State Key Laboratory of Polymer Materials Engineering of China, Polymer Research Institute, Sichuan University, Chengdu 610065, China.

[b] Institut National de la Recherche Scientifique-Énergie Materiaux et Télécommunications, Varennes, Quebec J3X 1S2, Canada

*Corresponding author. E-mail address: zhoutaopoly@scu.edu.cn (T. Zhou); shuhui@emt.inrs.ca (S. Sun)

1. Characterizations of copper oxalate (CuC_2O_4) and copper acetylacetonate [$Cu(acac)_2$]

1.1. Fourier transform infrared (FTIR) spectroscopy

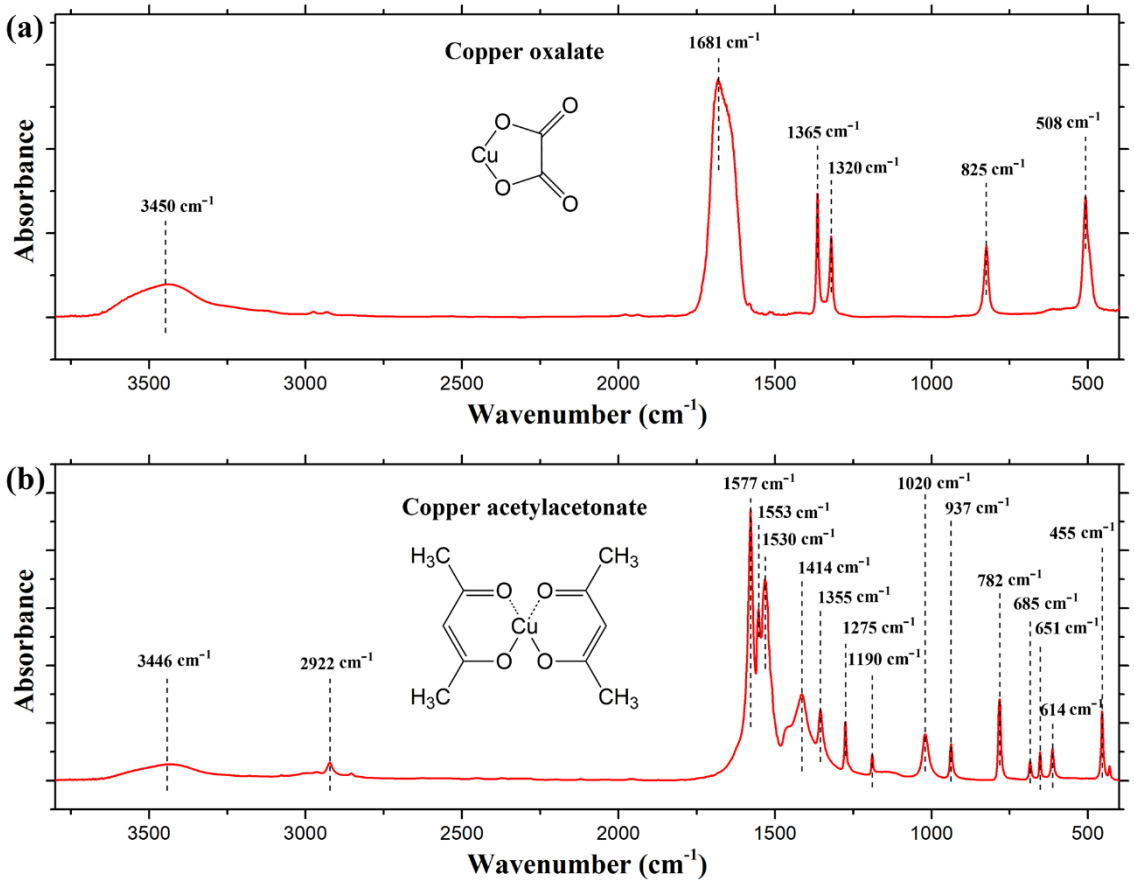

Figure S1. FTIR spectra in the region of 3800−400 cm^{-1}. **(a)** copper oxalate (CuC_2O_4); **(b)** copper acetylacetonate [$Cu(acac)_2$].

The formula of CuC_2O_4 consists of one copper cation attached to one oxalate anion. In **Figure S1(a)**, the broad bands at 3450 cm^{-1} is assigned to −OH stretching vibration, and the band around 1681 cm^{-1} is attributed to C=O stretching vibration. The peaks at 1365 cm^{-1} and 1320 cm^{-1} are assigned to the C−O stretching vibration of the coordinated oxalate group, and 825 cm^{-1} and 508 cm^{-1} are attributed to the vibrations of Cu−O.

The formula of $Cu(acac)_2$ consists of acetylacetonate anion forms a chelation ring by binding each oxygen atom with the copper cation. In **Figure S1(b)**, the broad bands at 3446 cm^{-1} is assigned to −OH stretching vibration, and the bands around 2922 cm^{-1} is attributed to C−H stretching vibration. The bands at 1577 cm^{-1}, 1553 cm^{-1}, and 1530 cm^{-1} are attributed to the C=C stretching vibration, and 1414 cm^{-1} and 1355 cm^{-1} are assigned to the C−H bending vibration. The peaks at 1275 cm^{-1}, 1190 cm^{-1}, 1020 cm^{-1}, and 937 cm^{-1} are

attributed to the C−O stretching vibration. The bands at 782 cm^{-1}, 685 cm^{-1}, 651 cm^{-1}, 614 cm^{-1}, and 455 cm^{-1} are assigned to the vibrations of Cu−O.

1.2. X-Ray photoelectron spectroscopy (XPS)

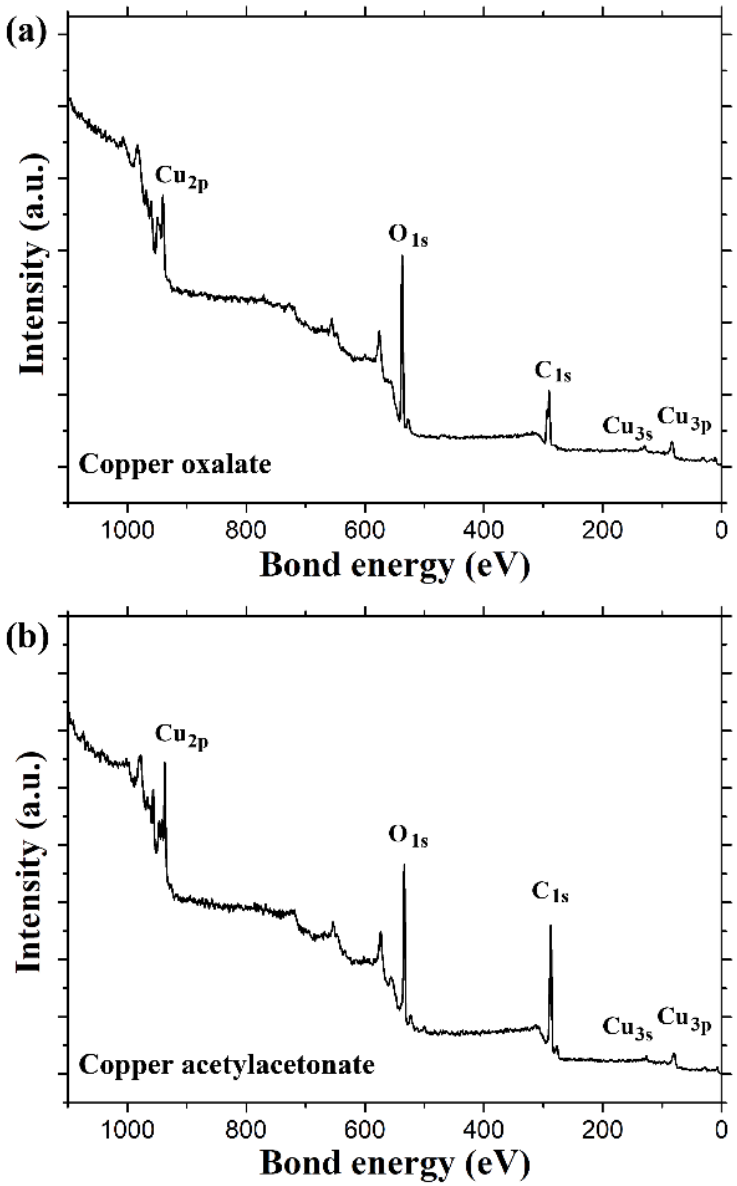

Figure S2. XPS survey spectra. **(a)** copper oxalate (CuC_2O_4); **(b)** copper acetylacetonate [$Cu(acac)_2$].

In **Figure S2**, X-Ray photoelectron spectroscopy (XPS) analysis was used to investigate the elemental compositions of CuC_2O_4 and $Cu(acac)_2$. From the survey spectra of XPS, it can be observed that both CuC_2O_4 and $Cu(acac)_2$ only exhibit absorption peaks of Cu, C, and O elements.

1.3. Powder X-ray diffraction (PXRD)

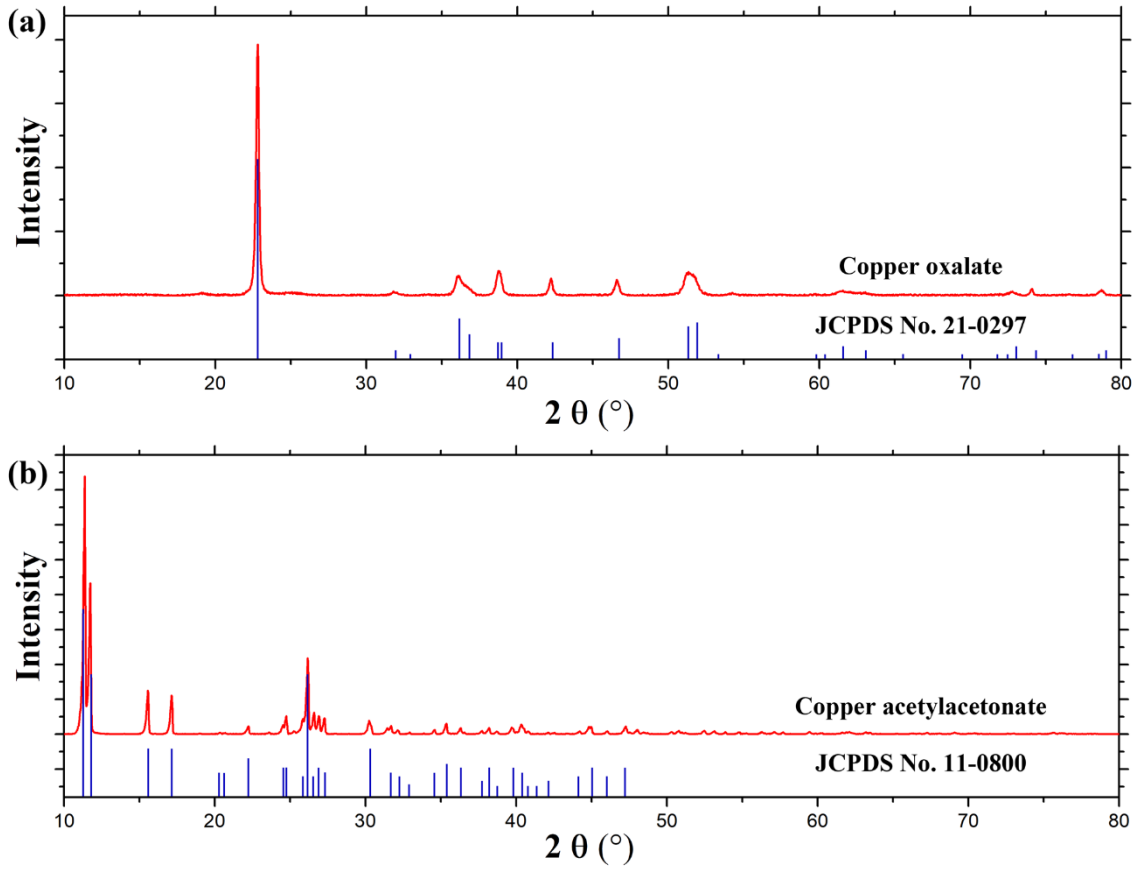

Figure S3. (a) PXRD pattern in red and reference PXRD peaks (represented as vertical blue bars) of the CuC_2O_4 (JCPDS card File No. 21-0297). **(b)** PXRD pattern in red and reference PXRD peaks (represented as vertical blue bars) of the $Cu(acac)_2$ (JCPDS card File No. 11-0800).

Figure S3 illustrates PXRD patterns of CuC_2O_4 and $Cu(acac)_2$, which are precisely matched with the JCPDS cards (File No. 21-0297 and File No. 11-0800), respectively. No additional diffraction peaks are observed, indicating the high purity of CuC_2O_4 and $Cu(acac)_2$.

1.4. Scanning electron microscopy (SEM)

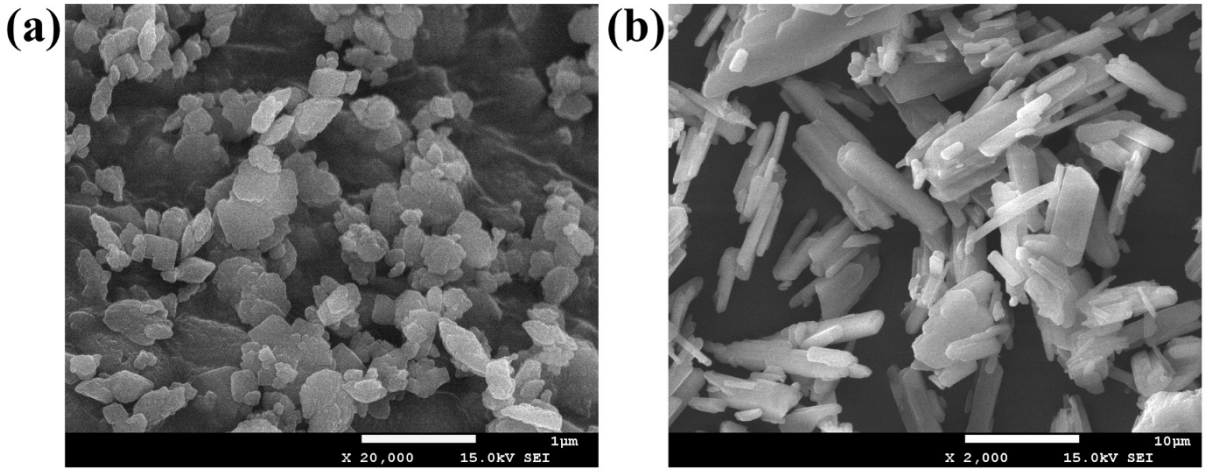

Figure S4. (a) SEM image of copper (II) oxalate (CuC_2O_4), scale bar: 1 µm. **(b)** SEM image of copper (II) acetylacetonate [$Cu(acac)_2$], scale bar: 10 µm.

From the SEM morphology observations, it can be seen that CuC_2O_4 is spherical particles **[Figure S4(a)]**, while the [$Cu(acac)_2$] rod-shaped particles **[Figure S4(b)]**.

1.5. Thermogravimetric (TG) analysis

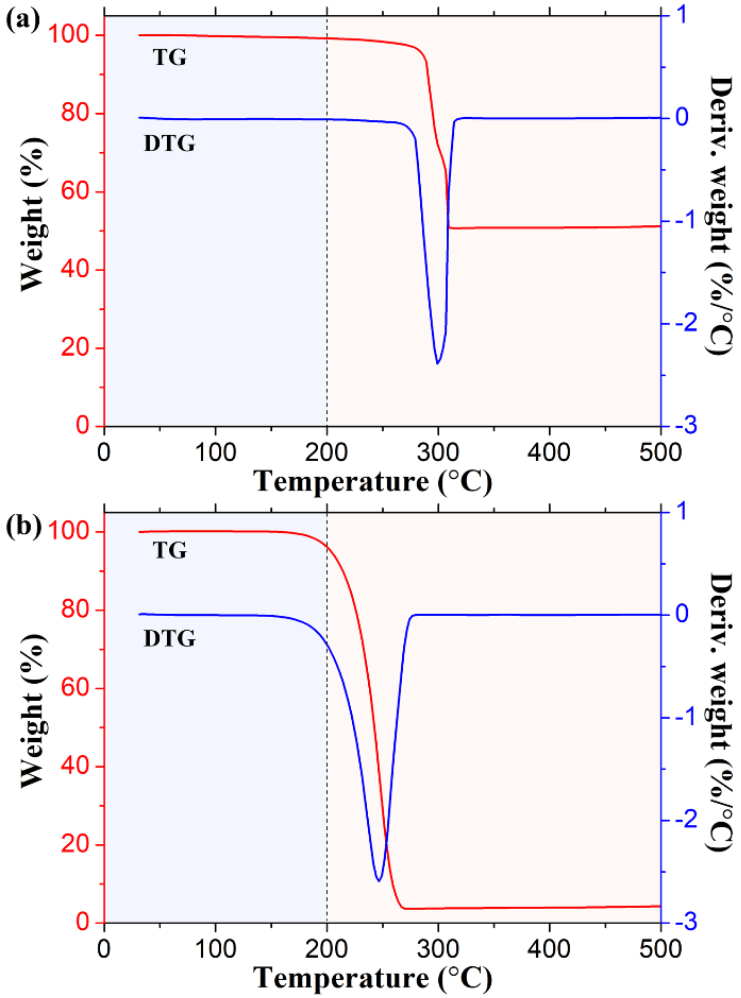

Figure S5. TG and DTG curves of samples upon heating from 30 °C to 500 °C at 10 °C/min under air atmosphere. **(a)** copper (II) oxalate (CuC_2O_4); **(b)** copper (II) acetylacetonate [$Cu(acac)_2$].

The TG analysis was carried out to investigate the thermal stability of CuC_2O_4 and [$Cu(acac)_2$]. Under plastic processing temperature below 200 °C, the CuC_2O_4 and $Cu(acac)_2$ can keep a good stability.

2. Contact angles

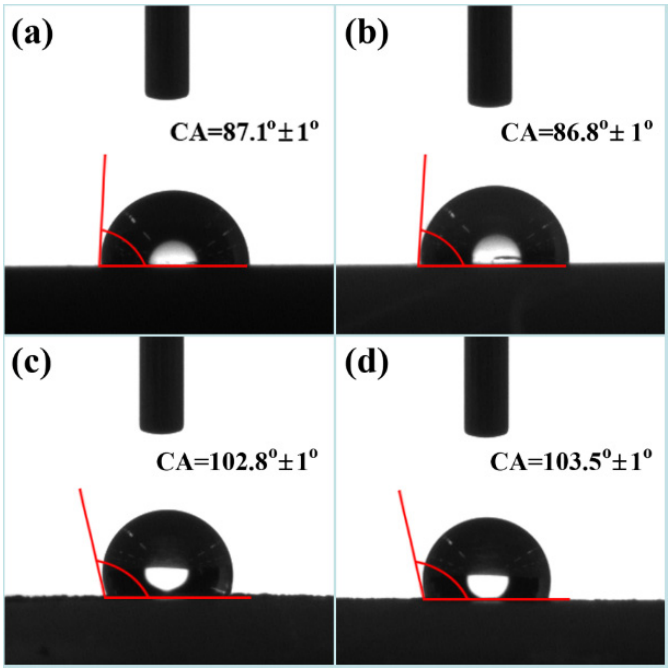

Figure S6. Surface contact angles of ABS composites before and after NIR pulsed laser irradiation. **(a)** ABS/CuC_2O_4 before laser irradiation; **(b)** ABS/$Cu(acac)_2$ before laser irradiation. **(c)** ABS/CuC_2O_4 after laser irradiation; **(d)** ABS/$Cu(acac)_2$ after laser irradiation.

3. UV-vis-IR spectroscopy

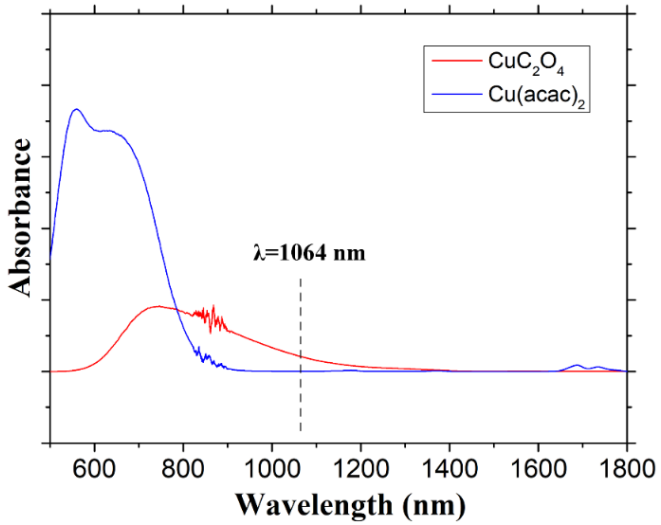

Figure S7. UV-vis-IR spectra of CuC_2O_4 and $Cu(acac)_2$ in the region of 500−1800 nm.

The UV-vis-IR measurements were carried out to investigate the absorption of CuC_2O_4 and $Cu(acac)_2$ at 1064 nm, which is corresponding to the wavelength of NIR laser used in our work. In **Figure S7**, it can be seen that the absorption of CuC_2O_4 is stronger than $Cu(acac)_2$ at 1064 nm.

4. Laser irradiation of neat CuC_2O_4 and $Cu(acac)_2$

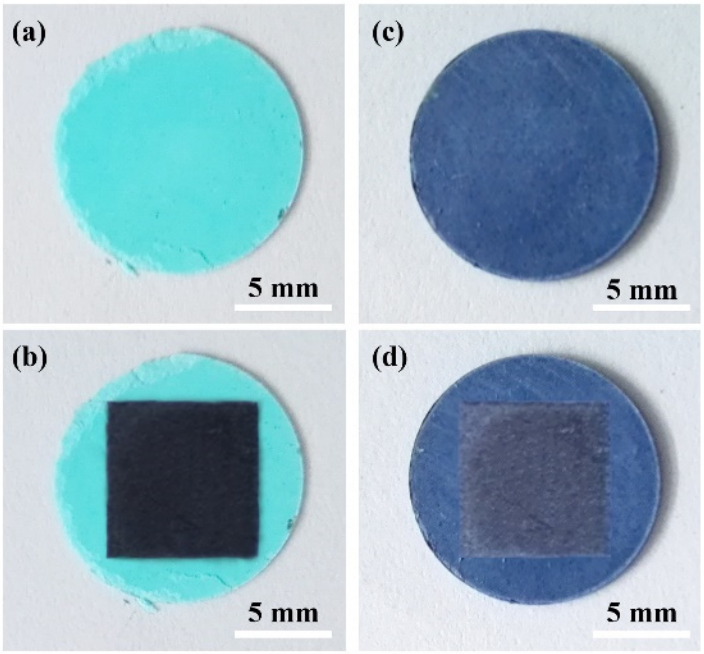

Figure S8. Neat CuC_2O_4 and $Cu(acac)_2$ before and after NIR pulsed laser irradiation. **(a)** CuC_2O_4 before laser irradiation; **(b)** CuC_2O_4 after laser irradiation. **(c)** $Cu(acac)_2$ before laser irradiation; **(d)** $Cu(acac)_2$ after laser irradiation. The laser parameters are 400 $mm \cdot s^{-1}$ (laser scanning speed), 8 W (laser power), and 60 kHz (laser pulse frequency).

5. XRD of the obtained copper layer on ABS/CuC_2O_4 and ABS/$Cu(acac)_2$

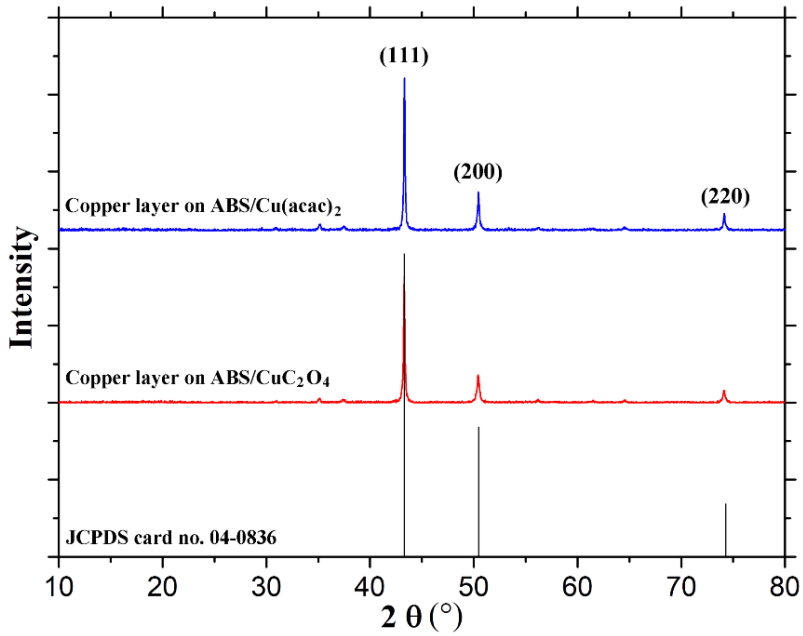

Figure S9. XRD patterns of the copper layer on ABS/CuC_2O_4 and ABS/$Cu(acac)_2$. The reference XRD peaks (represented as vertical black bars) of the Cu cubic structure (ICSD PDF no. 04-0836).

6. X-Ray photoelectron spectroscopy

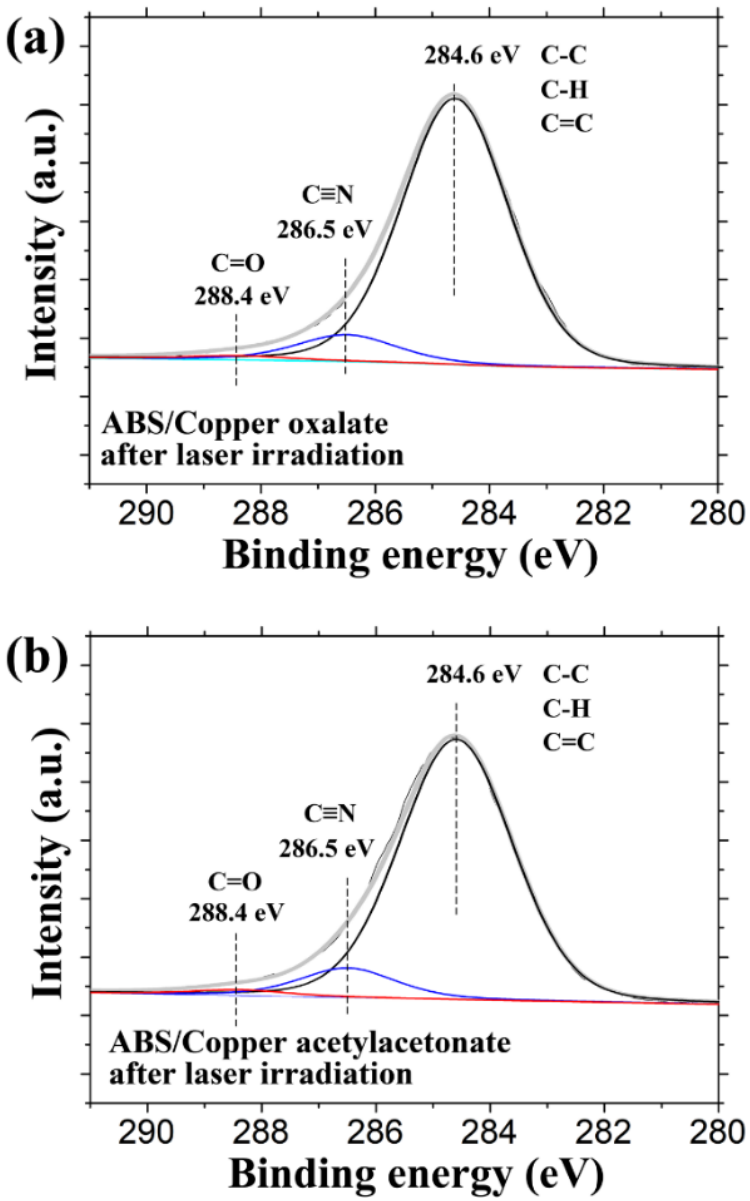

Figure S10. (a) High-resolution C 1s spectra of ABS/CuC_2O_4 after laser irradiation. **(b)** High-resolution C 1s spectra of ABS/$Cu(acac)_2$ after laser irradiation.

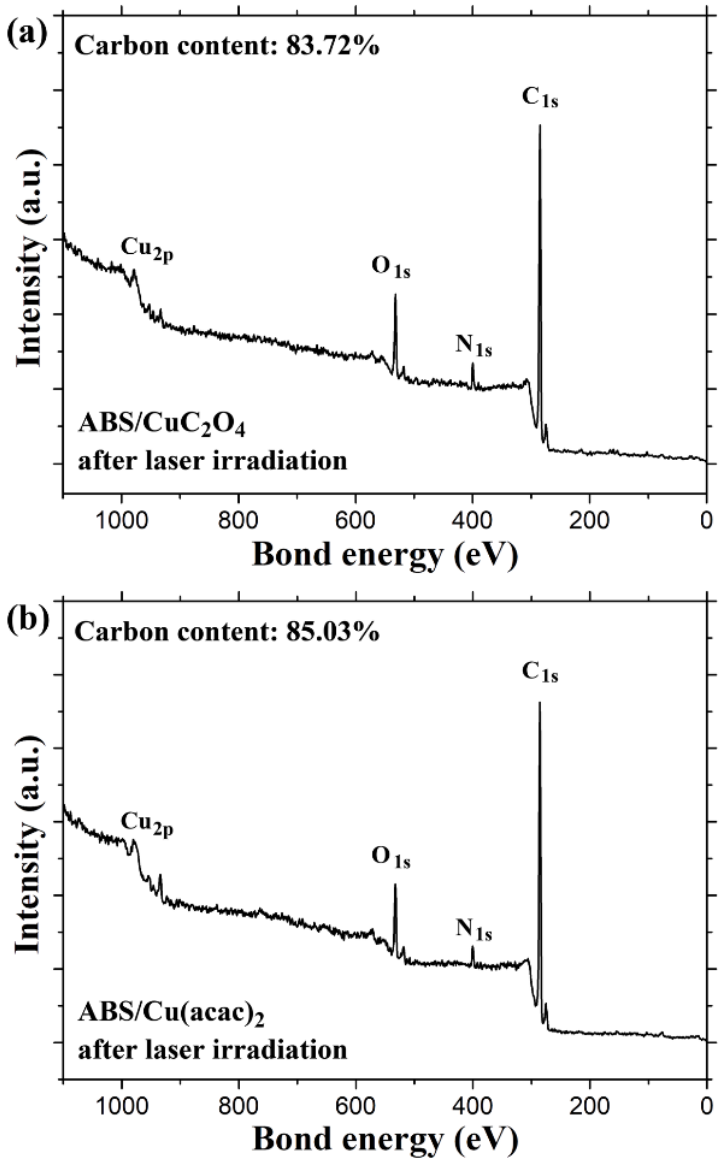

Figure S11. (a) XPS survey spectra of ABS/CuC_2O_4 after laser irradiation. **(b)** XPS survey spectra of ABS/$Cu(acac)_2$ after laser irradiation.

7. The narrowest conductive line on ABS/CuC_2O_4 and ABS/$Cu(acac)_2$

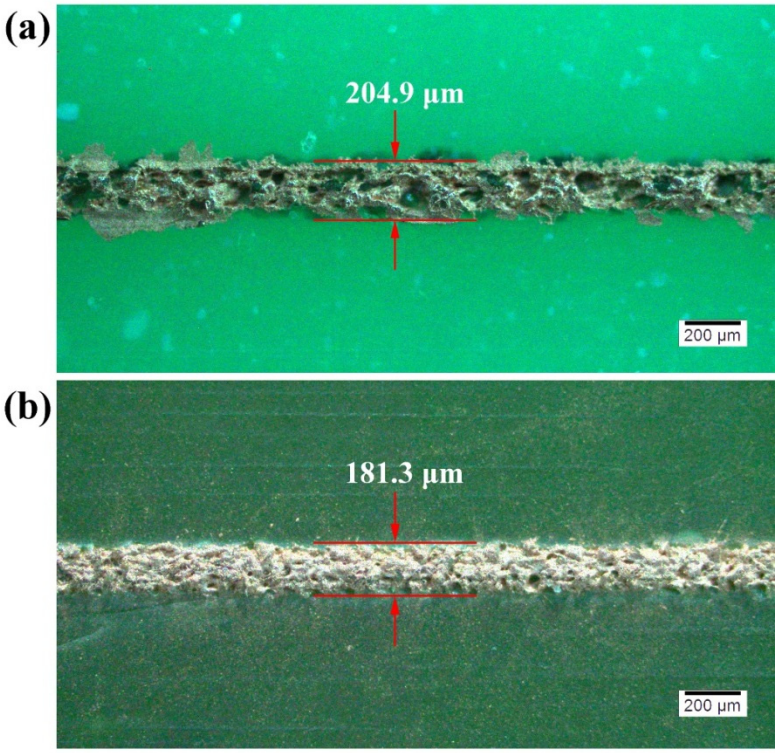

Figure S12. Optical microscope photographs of the narrowest conducting wires obtained, scale bar 200 µm. **(a)** ABS/CuC_2O_4; **(b)** ABS/$Cu(acac)_2$.

8. Scotch tape test of the copper layer on ABS/CuC_2O_4 and ABS/$Cu(acac)_2$

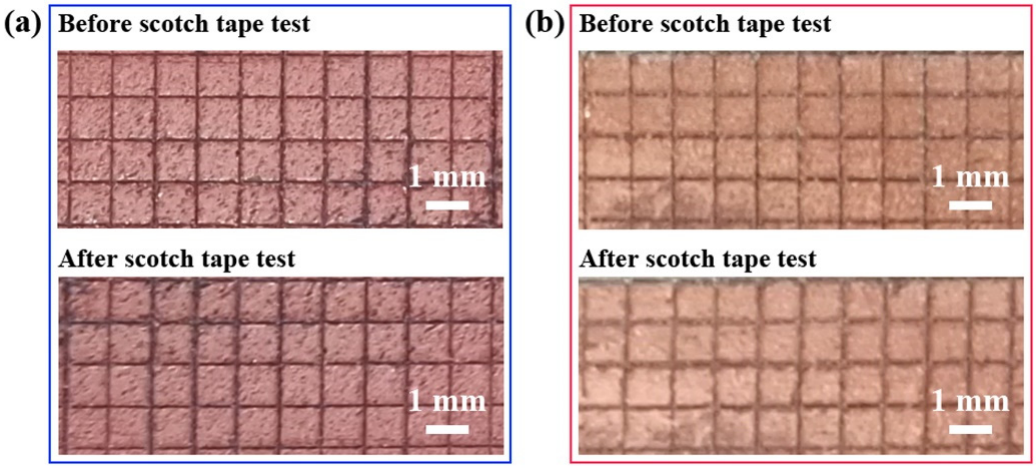

Figure S13. Scotch tape test of the obtained copper layer. **(a)** ABS/CuC_2O_4; **(b)** ABS/$Cu(acac)_2$.

According to the American Society for Testing and Materials (ASTM) D3359 (Scotch tape testing), the performance of mechanical adhesion between the obtained copper layer and polymer substrate was carried out *via* suddenly removing the pressure-sensitive adhesive tape (3M 600-HC33) tightly sticking on the 1 × 1 mm^2 crosshatched squares. The

mechanical adhesion is usually classified into 6 levels based upon the percentage of the area being removed, including 0B (be removed more than 65%), 1B (be removed 35−65%), 2B (be removed 15− 35%), 3B (be removed 5−15%), 4B (be removed less than 5%), and 5B (none of the squares be removed), respectively.

9. The optical microscope photograph of the IC chip

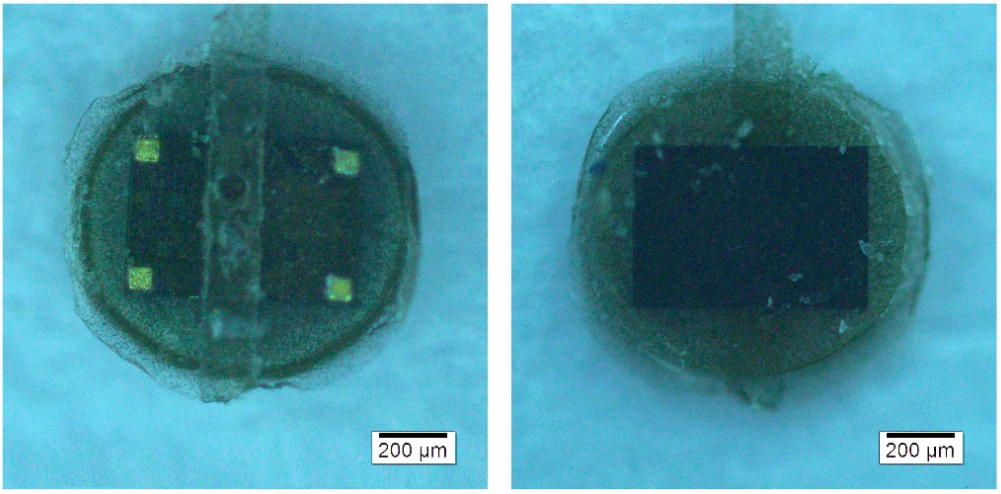

Figure S14. Front and back optical microscope photographs of the IC chip, scale bar 200 μm.

10. The conductivity of the copper layer on ABS/CuC_2O_4 and ABS/$Cu(acac)_2$

The following equation can calculate the conductivity of the circuit:

$$\rho = \frac{L}{RS}$$

where ρ is the conductivity, and R is the resistance. The L is the circuit length, and S is the cross-sectional area of the circuit.

For ABS/CuC_2O_4, after 30 min electroless copper plating, the length, width, and thickness of the copper circuit are 21×10^{-3} m, 2×10^{-3} m, and 6.35×10^{-6} m, respectively. The corresponding resistance is 0.135 Ω.

The specific calculations are below:

$$\rho = \frac{L}{RS} = \frac{21 \times 10^{-3}}{0.135 \times 2 \times 10^{-3} \times 6.35 \times 10^{-6}} = 1.22 \times 10^{7}\ \Omega^{-1} \cdot m^{-1}$$

For ABS/$Cu(acac)_2$, after 30 min electroless copper plating, the length, width, and thickness of the copper circuit are, 21×10^{-3} m, 2×10^{-3} m, and 5.61×10^{-6} m, respectively. The corresponding resistance is 0.118 Ω.

The specific calculations are below:

$$\rho = \frac{L}{RS} = \frac{21 \times 10^{-3}}{0.118 \times 2 \times 10^{-3} \times 5.61 \times 10^{-6}} = 1.58 \times 10^{7}\ \Omega^{-1} \cdot m^{-1}$$

Supplementary Video S1 and S2 Captions

Video S1

Selective laser activation of the ABS/$Cu(acac)_2$ composites with laser wavelength 1064 nm, laser scanning speed 400 $mm \cdot s^{-1}$, laser power 8 W, and laser pulse frequency 60 kHz. The video demonstrates the laser activation for patterns of near field communication (NFC) with a high resolution and sharp edges *via* the NIR laser system.

Video S2

The writing and identification process of the near-field communication (NFC) device by using a smartphone. Before writing information, the IC chip is empty. Then, the website message of "Sichuan University" is stored to the IC chip *via* NFC between the functional tag and an NFC-enabled smartphone. After that, the website message is conveniently retrieved with the smartphone also *via* NFC.